Simple and efficient Method of Lines based algorithm for modelling of erbium doped Q-switched fluoride fiber lasers

SLAWOMIR SUJECKI*

George Green Institute for Electromagnetics Research, University of Nottingham, University Park, NG7 2RD Nottingham, UK and Department of Telecommunications and Teleinformatics, Faculty of Electronics, Wroclaw University of Science and Technology, Wyb. Wyspianskiego 27, 50-370 Wroclaw, Poland
**Corresponding author: slawomir.sujecki@nottingham.ac.uk*

Received XX Month XXXX; revised XX Month, XXXX; accepted XX Month XXXX; posted XX Month XXXX (Doc. ID XXXXX); published XX Month XXXX

An improved algorithm based on the method of lines for modelling of Q-switched fluoride glass based erbium doped fiber lasers is presented. The algorithm uses finite difference method to reduce partial differential equations to a set of ordinary differential equations. Unlike the method of characteristics the ratio of the temporal and spatial step is not fixed. Thus computationally efficient algorithms with an adaptive step control for the solution of a set of ordinary differential equations can be directly applied. The performance of the improved algorithm against the standard one is compared. The results obtained show that the improved algorithm is significantly more computationally efficient.

OCIS codes: *(140.3510) Lasers, fiber; (140.3540) Lasers, Q-switched.*

http://dx.doi.org/10.1364/AO.99.099999

1. INTRODUCTION

Mid Infrared (MIR) light sources have many applications in medicine, environment monitoring, and defense. For these applications a variety of MIR sources have been developed. Of particular importance for practical applications are laser sources. Many types of MIR lasers have been developed: gas lasers, solid state lasers, fiber lasers and quantum cascade lasers. The fiber lasers when compared with other technologies are robust, reliable, compact, and offer high quality of the output beam. So far wavelengths as long as 3.9 μm have been achieved by fiber lasers using liquid nitrogen cooled ZBLAN fiber doped with holmium ions [1]. In recent years the development of the erbium doped fluoride fiber laser sources turned out to be particularly successful [2-8]. These lasers are typically operating at approximately 3 μm, operate at room temperature and have a simple pumping mechanism, which relies on the use of standard 980 nm pump semiconductor lasers that are robust, reliable and can deliver high power at a relatively low cost. Further, erbium doped fluoride fibers are commercially available from several manufacturers at a moderate cost per meter. So far, the Er^{3+} doped fiber lasers have been demonstrated to be capable of operating at room temperature with output wavelength as long as 3.6 μm [7]. Under CW (continuous wave) operation the Er^{3+} doped fiber lasers have reached the output power of 24 W using a fiber immersed in the fluorocarbon liquid in a configuration using bulk optics elements [2] while in all fiber, passively cooled configuration 20 W was obtained [4]. The slope efficiency of CW erbium doped fluoride fiber lasers has reached so far 51 % [5]. Also a number of Q-switched pulsed lasers were developed using erbium doped ZBLAN fibers. The highest average power achieved so far in using Q-switching is 12 W with the pulse energy up to 0.1 mJ [3] while the highest peak power achieved so far is 10 kW with the pulse energy exceeding 0.5 mJ [6]. Finally, it is noted that the ZBLAN fibers have been successfully applied in ultrafast fiber lasers [8].

With the increasing number of successfully realized various erbium doped fluoride fiber lasers the design and optimization becomes increasingly important, especially when attempting to convert erbium doped fluoride fiber lasers from experimental laboratory setups into commercial products that can compete on the market with other types of lasers. The design of fluoride glass based erbium doped fiber lasers has therefore attracted significant attention. Several models were developed for modelling erbium doped fluoride fiber lasers and amplifiers [9-14]. These laser models rely on solving the rate equations and the propagation equations for the pump and signal waves in the time domain and are closely related to models used for time domain simulations of Q-switched silica glass based fiber lasers [15] and Raman fiber amplifiers [16]. In [9-14] the partial differential equations (PDEs) that describe the propagation of forward and backward travelling waves for the pump and signal in these models were reduced to a set of ordinary differential equations (ODEs) using the method of characteristics (MOC). However, for MOC the spatial and temporal step ratio is fixed and has to be kept at a constant value equal to the optical wave group velocity for the transient results to preserve their physical meaning. This significantly affects the algorithm efficiency since the

benefit of applying adaptive step algorithms for the integration of the ODEs cannot be fully taken advantage of. Therefore, in this contribution a different approach is pursued. The finite difference method and the method of lines (FD-MOL) is used to reduce the PDEs for the forward and backward travelling waves to a set of ODEs. It is shown that this allows a direct application of computationally efficient algorithms with an adaptive step control for the integration of ODEs, which are readily available from the standard numerical libraries. Thus the model development turns into a comparatively simple task. A standard first order accurate algorithm is presented that was adapted from the field of semiconductor laser modelling [17]. Then the concept of the Extended Taylor Series (ETS) [18-21] is applied to derive second order finite difference (FD) approximations and develop a FD-MOL algorithm for modelling Q-switched erbium doped fluoride glass fiber lasers. It is shown that the FD-MOL using second order finite difference approximations is significantly more efficient than the one using the first order approximations.

The paper is divided into four sections. In second section the equations are provided that describe the level populations' distributions and the distribution of the photon density in the cavity and provide the derivation of the first and second order FD approximations. In the third section the results are discussed and a concise summary is provided in the last section.

2. THEORY

Let's consider a simple fiber laser cavity pumped at z = 0 with the output signal collected from the other end of the fiber at $z = L_{fib}$ (Fig.1a). The evolution of the pump and signal powers (P_p and P_s respectively) is described by the equations [9, 11, 14]:

$$\left(\frac{\partial}{\partial z}+\frac{1}{v_g}\frac{\partial}{\partial t}\right)P_p^+=\left(g_p-\alpha_p\right)P_p^+ \qquad \textbf{(1a)}$$

$$\left(-\frac{\partial}{\partial z}+\frac{1}{v_g}\frac{\partial}{\partial t}\right)P_p^-=\left(g_p-\alpha_p\right)P_p^- \qquad \textbf{(1b)}$$

$$\left(\frac{\partial}{\partial z}+\frac{1}{v_g}\frac{\partial}{\partial t}\right)P_s^+=\left(g_s-\alpha_s\right)P_s^+ \qquad \textbf{(1c)}$$

$$\left(-\frac{\partial}{\partial z}+\frac{1}{v_g}\frac{\partial}{\partial t}\right)P_s^-=\left(g_s-\alpha_s\right)P_s^- \qquad \textbf{(1d)}$$

The partial differential equations 1 are solved subject to the following boundary conditions:

$$P_p^+\left(z=0\right)=R_p\left(z=0\right)P_p^-\left(z=0\right)+\left(1-R_p\left(z=0\right)\right)P_{pump} \qquad \textbf{(2a)}$$

$$P_p^-\left(z=L_{fib}\right)=R_p\left(z=L_{fib}\right)P_p^+\left(z=L_{fib}\right) \qquad \textbf{(2b)}$$

$$P_s^+\left(z=0\right)=R_s\left(z=0\right)P_s^-\left(z=0\right) \qquad \textbf{(2c)}$$

$$P_s^-\left(z=L_{fib}\right)=R_s\left(z=L_{fib}\right)P_s^+\left(z=L_{fib}\right) \qquad \textbf{(2d)}$$

where L_{fib} is the fiber length, R_p and R_s is the facet power reflectivity for the pump and signal waves, respectively, while P_{pump} stands for the pump power launched at the fiber. First the cavity is unfolded following on the concepts outlined in [22]. The concept of unfolding the cavity is illustrated in Fig.1b and Fig.1c. In the standard approach the computational domain for forward and backward propagating waves is separate. When unfolding the cavity both domains are combined and the reflection coefficient is effectively replaced by the transmission coefficient of the same value. For the unfolded cavity one obtains the following equations for the pump and signal waves:

$$\left(\frac{\partial}{\partial z}+\frac{1}{v_g}\frac{\partial}{\partial t}\right)P_p^+=\left(g_p-\alpha_p\right)P_p^+ \qquad \textbf{(3a)}$$

$$\left(\frac{\partial}{\partial z}+\frac{1}{v_g}\frac{\partial}{\partial t}\right)P_p^-=\left(g_p-\alpha_p\right)P_p^- \qquad \textbf{(3b)}$$

$$\left(\frac{\partial}{\partial z}+\frac{1}{v_g}\frac{\partial}{\partial t}\right)P_s^+=\left(g_s-\alpha_s\right)P_s^+ \qquad \textbf{(3c)}$$

$$\left(\frac{\partial}{\partial z}+\frac{1}{v_g}\frac{\partial}{\partial t}\right)P_s^-=\left(g_s-\alpha_s\right)P_s^- \qquad \textbf{(3d)}$$

So, the equations for forward and backward propagating waves have the same form, which reduces the amount of algebra necessary for deriving the finite difference approximations. When using the unfolded cavity approach one needs to map appropriately the backward propagating wave onto the domain of the level populations (Fig.1c – dashed lines).

In order to derive finite difference approximations for the spatial derivatives in (3) first a longitudinal discretization within the computational domain (Fig.1c) is introduced. At z = 0 the sample of signal or pump power for the forward propagating wave is not held since it is related through the boundary conditions (2) with the value of the power for the backward propagating wave (this is marked schematically by a black disc and a circle in Fig.1c). Similarly, the value of the power for the forward propagating wave is stored only at $z = L_{fib}$. Keeping this in mind the Extended Taylor Series (ETS) is derived for the part of the computational domain containing the discontinuity. Assuming that the value of the pump power on the left hand side (LHS) of the discontinuity is related to the value of the power at the right hand side (RHS) via (c.f. equations 2):

$$P^+=RP^-+T_0;\quad T_0=\left(1-R\right)P_{pump} \qquad \textbf{(4a)}$$

one obtains the following continuity conditions for the spatial derivatives of the power:

$$\left.\frac{\partial P}{\partial z}\right|^+=R\left.\frac{\partial P}{\partial z}\right|^-+T_1;\quad T_1=\left(\Gamma g-\alpha\right)\left(1-R\right)P_{pump} \qquad \textbf{(4b)}$$

$$\left.\frac{\partial^2 P}{\partial z^2}\right|^+=R\left.\frac{\partial^2 P}{\partial z^2}\right|^-+T_2;\quad T_2=\left(\frac{\partial T_1}{\partial z}-\frac{1}{v_g}\frac{\partial T_1}{\partial t}\right)+\left(\Gamma g-\alpha\right)T_1 \qquad \textbf{(4c)}$$

It is noted that for the signal power T_0, T_1 and T_2 are equal to zero.

For higher order derivatives one obtains a generic form of the continuity condition:

$$\left.\frac{\partial^n P}{\partial z^n}\right|^+=R\left.\frac{\partial^n P}{\partial z^n}\right|^-+T_n \qquad \textbf{(4d)}$$

a)

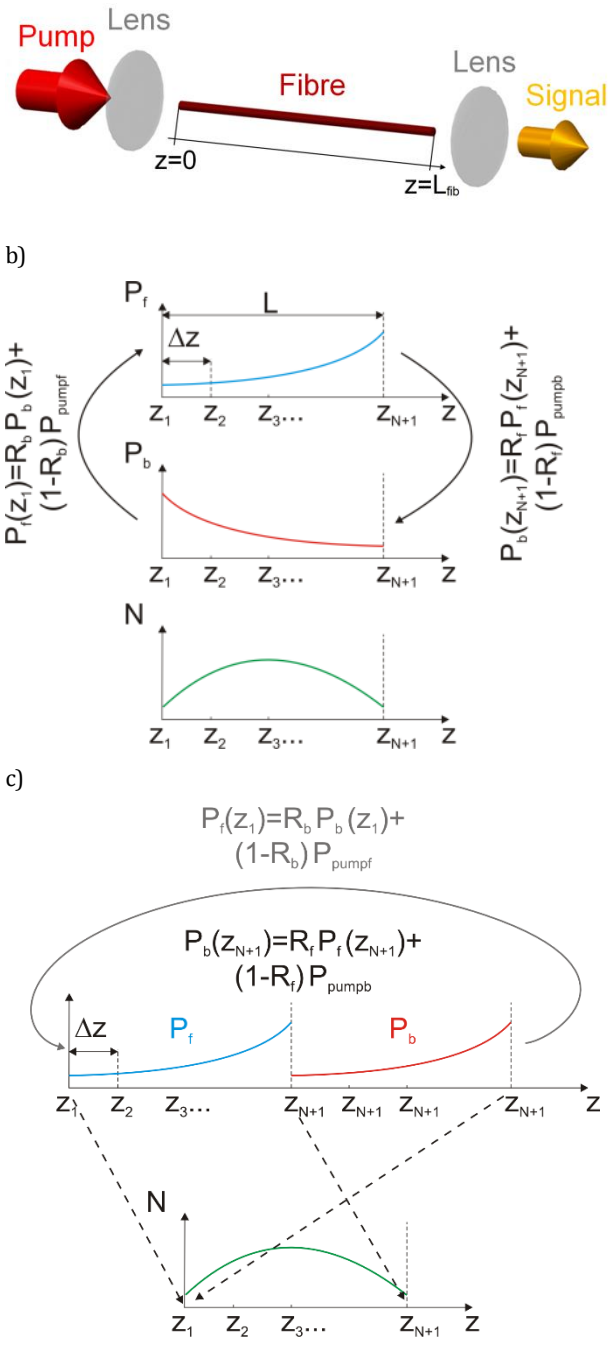

Fig. 1. Schematic diagram of the fiber laser cavity -a); the distribution and mapping of the finite difference sampling points within the computational domain before -b) and after unfolding the cavity -c).

The exact form of the ETS relating the power values at two distinct finite difference nodes depends on the position of the discontinuity within the stencil. With using up to three nodes one can have three possible situations (Fig.2). Consistently with Fig.1c the pump and signal power samples are kept to the left of the position of discontinuity and place the discontinuity coincidently with a finite difference node (Fig.2). Thus following the methodology outlined in [20] one obtains the following ETS approximation for Fig.2a:

$$RP_{-2} = e^{-2\Delta z D} P_0 - T_0 \quad \textbf{(5a)}$$

$$P_{-1} = e^{-\Delta z D} P_0 \quad \textbf{(5b)}$$

where D is the differentiation operator: d/dz. Similarly, for Fig.2b one has:

$$RP_{-2} = e^{-2\Delta z D} P_0 - \sum_{n=0}^{\infty} (-1)^n \Delta z^n T_n \quad \textbf{(5c)}$$

$$RP_{-1} = e^{-\Delta z D} P_0 - T_0 \quad \textbf{(5d)}$$

and for Fig.2c:

$$P_{-2} = e^{-2\Delta z D} P_0 \quad \textbf{(5e)}$$

$$P_{-1} = e^{-\Delta z D} P_0 \quad \textbf{(5f)}$$

Using expansions 5 the following backward finite difference approximations are obtained:

$$\left.\frac{dP}{dz}\right|_0 = \frac{1}{2\Delta z}(3P_0 - 4RP_{-1} + RP_{-2}) + O(\Delta z^2) + \frac{T_0}{2\Delta z} \quad \textbf{(6a)}$$

for Fig.2a, for Fig.2b:

$$RP_{-2} = e^{-2\Delta z D} P_0 - T_0 \quad \textbf{(6b)}$$

$$P_{-1} = e^{-\Delta z D} P_0 \quad \textbf{(6c)}$$

and for Fig.2c:

$$\left.\frac{dP}{dz}\right|_0 = \frac{1}{2\Delta z}(3P_0 - 4P_{-1} + P_{-2}) + O(\Delta z^2) \quad \textbf{(6d)}$$

$$\left.\frac{dP}{dz}\right|_0 = \frac{1}{\Delta z}(P_0 - P_{-1}) + O(\Delta z) \quad \textbf{(6e)}$$

where $O(\Delta z)$ designates terms containing first and higher powers of Δz while $O(\Delta z^2)$ terms containing second and higher powers of Δz.

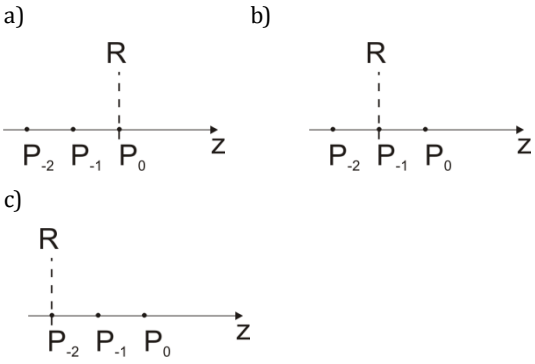

Fig. 2. Schematic diagram showing the position of the discontinuity within the three point backward finite difference stencil: first node -a); second node -b) and third node -c).

Equations 6a, 6b and 6d give 2nd order accuracy whilst equations 6c and 6e are 1st order accurate. It is also noted that equations 6d and 6e are the standard finite difference approximations, which apply at all nodes when the finite difference stencil does not cross a discontinuity position.

Using the finite difference approximations 6 one can convert partial differential equations 3 into a set of ordinary differential equations (ODEs). Due to the presence of strong oscillations during the switch on process [12] ODE integration schemes suitable for stiff systems need to be applied.

3. RESULTS

An erbium ion model is considered that includes 5 distinct energy levels (Fig.3) [14]. The levels $^4F_{7/2}$, $^4H_{11/2}$ and $^4S_{3/2}$ are considered to be in a thermal equilibrium due to phonon coupling and hence are represented by one level – N_4. Similarly, the levels $^4I_{9/2}$ and $^4I_{11/2}$ are represented by the level N_2, which is at the same time the upper lasing level. The following equations describe the level population dynamics (c.f. Fig.3):

$$\begin{aligned}
\frac{\partial N_4}{\partial t} &= W_{22}N_2^2 - \frac{N_4}{\tau_4} \\
\frac{\partial N_3}{\partial t} &= \frac{\beta_{43}N_4}{\tau_4} - \frac{N_3}{\tau_3} \\
\frac{\partial N_2}{\partial t} &= R_{GSA} - R_{SE} + \sum_{i=3}^{4}\frac{\beta_{i2}N_i}{\tau_i} - \frac{N_2}{\tau_2} - 2W_{22}N_2^2 + W_{11}N_1^2 \\
\frac{\partial N_1}{\partial t} &= R_{SE} + \sum_{i=2}^{4}\frac{\beta_{i1}N_i}{\tau_i} - \frac{N_1}{\tau_1} - 2W_{11}N_1^2 \\
\frac{\partial N_0}{\partial t} &= -R_{GSA} + \sum_{i=1}^{4}\frac{\beta_{i0}N_i}{\tau_i} + W_{22}N_2^2 + W_{11}N_1^2
\end{aligned} \quad \textbf{(7)}$$

It is assumed that the up-conversion to all other levels is negligible and hence:

$$N_0 + N_1 + N_2 + N_3 + N_4 = N_{Er} \quad \textbf{(8)}$$

where N_{Er} is the erbium ion dopant concentration. The symbols τ_i denote level i lifetime and β_{ij} are the branching ratios for the levels i and j. W_{11} and W_{22} denote the coefficients for energy transfer upconversion from the $^4I_{13/2}$ and $^4I_{11/2}$ energy levels, respectively [9]. The ground state absorption rate and the stimulated emission rate are calculated from [9]:

$$R_{GSA} = \frac{\lambda_p \Gamma_p \sigma_{GSA}}{hcA_{eff}} N_0 \left(P_p^+ + P_p^-\right) \quad \textbf{(9a)}$$

$$R_{SE} = \frac{\lambda_s \Gamma_s \sigma_{se}}{hcA_{eff}} \left(b_2 N_2 - \frac{g_2}{g_1} b_1 N_1\right)\left(P_s^+ + P_s^-\right) \quad \textbf{(9b)}$$

When solving equations 7 in the time domain one needs to keep in mind that the initial values of level populations need to satisfy the condition 8 in order to obtain a physically meaningful solution. Tables 1 and 2 list the modelling parameters [9]. The branching ratios were slightly adjusted when compared with [9] so that they add up to 1. This is relevant to the consistency of the time domain calculations.

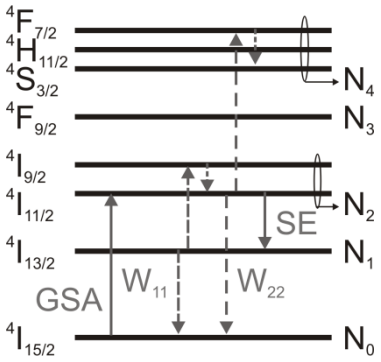

Fig. 3. Schematic diagram of the energy level model used in the simulations.

Table 1 Modelling parameters

parameter	Unit	value
b_1/b_2		0.1/0.16
W_{11}	m^3/s	$1x10^{-24}$
W_{22}	m^3/s	$0.3x10^{-24}$
λ_p	m	$976x10^{-9}$
λ_s	m	$2.8x10^{-6}$
σ_{GSA}	m^2	$2.1x10^{-25}$
σ_{SE}	m^2	$4.5x10^{-25}$
N_{Er}	$1/m^3$	$9.6x10^{26}$
L	m	2.5
Γ_p		0.009
Γ_s		1.0
α_p	1/m	$23x10^{-3}$
α_s	1/m	$3.0x10^{-3}$
$R_p(z=0)$		0
$R_p(z=L)$		0.04
$R_s(z=0)$		0.96
$R_s(z=L)$		0.04
A_{eff}	m^2	$314x10^{-12}$

Table 2 Branching ratios and level lifetimes

parameter	Unit	value
τ_1	ms	9.0
τ_2	ms	6.9
τ_3	μs	10
τ_4	μs	120
β_{21}, β_{20}		0.37, 0.63
β_{32}, β_{31}, β_{30}		0.99, 0.0, 0.01
β_{43}, β_{42}, β_{41}, β_{40}		0.85, 0.006, 0.004, 0.14

First the calculation of the steady state solution using the developed time domain model is discussed. The steady state solution provides a self-consistent initial state, which needs to be calculated before the shape of Q-switched pulses can be obtained numerically. For this purpose first the reference values of the output signal power are calculated using the steady state model based on the relaxation method (RM) [23]. The calculated values of the output power at four selected values of pump power are given in Table 3 and are believed to be accurate on twelve digital places. Also in order to shorten the time domain calculation time RM is used to calculate the initial signal and pump power distributions and level populations for the time domain (TD) model. The simulation time was selected to be equal to 30 ms, i.e. several times larger than the upper state radiative life time. It is also

noted that all calculations have been carried on a PC using a single processor clocked at 3.4 GHz within Matlab programming environment.

Table 3 Reference values of the output power and the CPU time required to calculate them

Pump power(z=0)/W	Output power ($z=L_{fib}$) /W	CPU time/s
5	1.39527600015	78.76
10	3.11902141885	85.94
15	4.85305182935	86.19
20	6.55663433930	84.27

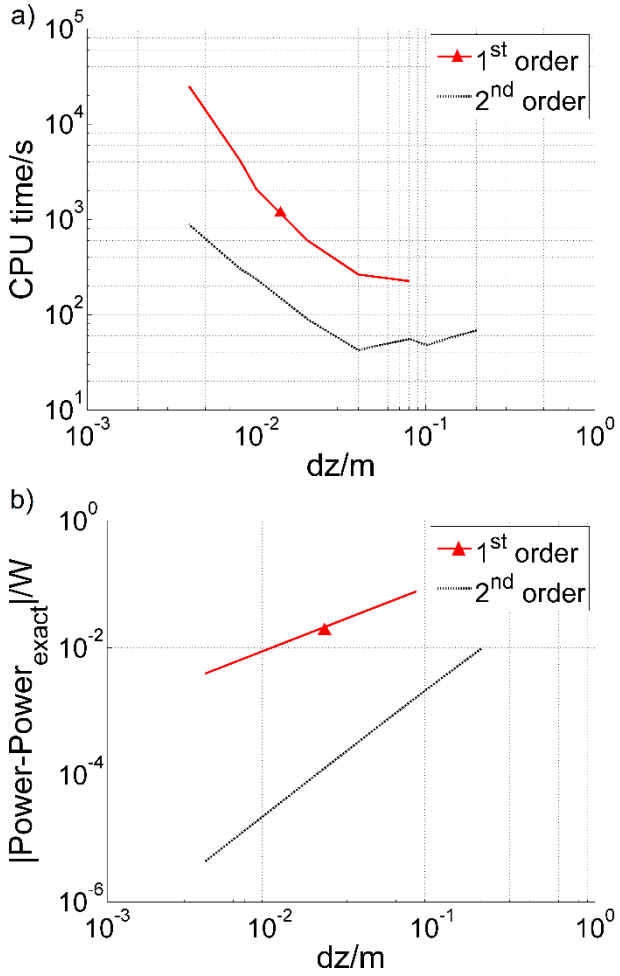

Fig. 4. Dependence of the CPU time -a) and the absolute error -b) on the spatial step size for the calculation of the steady state solution at 5 W input pump power for the 1st and 2nd order FD-MOL. This results were obtained for t = 30 ms.

Fig.4a shows the dependence of the CPU time needed to complete the TD simulations using the 1st and 2nd order FD approximation on the spatial discretization step. The CPU time for the 1st order method is significantly larger than in the case of 2nd order FD-MOL. Fig.4b shows the dependence of the absolute error, which was calculated using the reference values from Table 3, on the spatial discretization step. These results show that the 2nd order FD-MOL achieves much lower values of the absolute error than the 1st order FD-MOL. Also the inclination of the lines representing the error values for both methods is different. Table 4 shows the values for the error line inclination calculated at 4 values of the pump power. These results confirm that the derived FD approximations show truly 1st and 2nd order accuracy as expected. Lastly, one might find it surprising, that it takes more CPU time to obtain the results using the 1st order method when compared with the 2nd order method. The explanation of this fact can be extracted from the results presented in Fig.5. One can observe the presence of very strong oscillations in the dependence of the signal power on time (Fig.5d). It is also noted that the results shown in Fig.5e confirm that even though the level $^4I_{11/2}$ has a longer life time than that of the level $^4I_{13/2}$ the population inversion can still be achieved. This is due to the fact that in heavily erbium ion doped ZBLAN glass the energy transfer upconversion process ($^4I_{13/2}$,$^4I_{13,2}$) -> ($^4I_{15/2}$,$^4I_{9/2}$) is faster than ($^4I_{11/2}$,$^4I_{11,2}$) -> ($^4I_{15/2}$,$^4F_{7/2}$) [14].

Fig.6. shows the results from Fig.5d in magnification. The oscillations for the signal power are very strong. For an adaptive step ODE algorithm in order to preserve the low value of the set error tolerance whilst performing integration over these oscillations the time step has to be kept very small. This results in a long calculation time. For comparison Fig.7 shows the results obtained using the second order FD-MOL. There are only tiny oscillations of the signal power, which can be seen in more detail in Fig.8. An adaptive step ODE solver can perform the integration in such case with much longer time step and hence much shorter calculation time in the case of the 2nd order FD-MOL. The cause of strong oscillations in the case of the 1st order FD-MOL is its low accuracy and the fact that the accurate solution calculated by RM is used as an initial seed. Since the steady state solution of the 1st order FD-MOL differs significantly from the accurate one calculated by RM, it is perceived as a strong deviation from the steady state equilibrium intrinsic to the 1st order FD-MOL. Since 2nd order FD-MOL is significantly more accurate the accurate solution calculated using RM differs much less from the intrinsic steady state solution of the 2nd order FD-MOL. Hence, the time dependence of the signal power during the transition has much less structure. Finally, to avoid any confusion it is noted that the transition observed in Fig.6 and Fig.8 is a numerical artefact essentially caused by the discrepancies between the numerical solution of the steady state model and the numerical solutions of the time domain models.

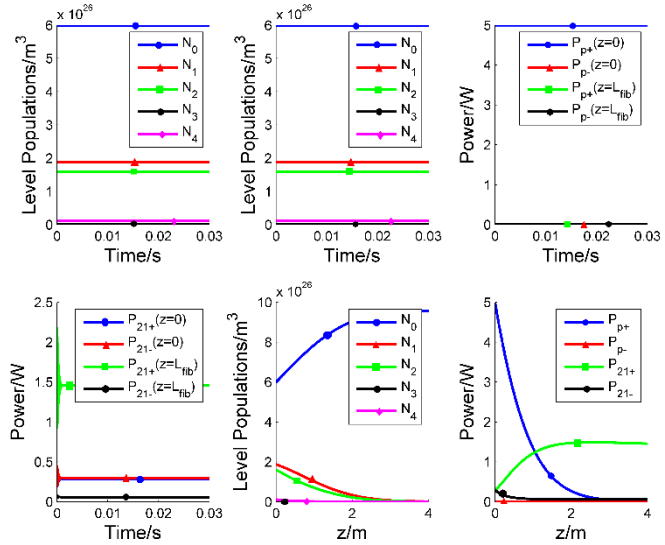

Fig. 5. Dependence on time of the level populations -a) and -b) and the pump -c) and signal power -d) at selected longitudinal positions; the final distribution of the level populations -e) and of pump and signal power -f) obtained for t = 30 ms. These results were calculated at 5 W input pump power using the 1st order FD-MOL.

Table 4 Finite difference approximation order extracted from the simulation results

Pump power/W	1st order	2nd order
5	0.996	1.973
10	0.997	1.998
15	0.997	2.026
20	0.995	2.044

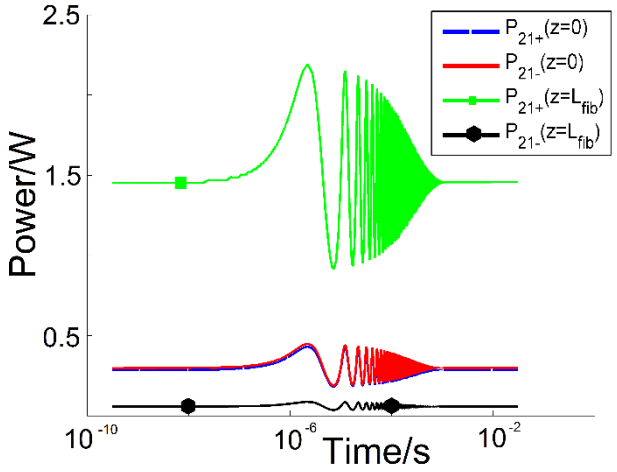

Fig. 6. Dependence of the signal power on time at selected longitudinal positions within the cavity. These results were calculated at 5 W input pump power using the 1st order FD-MOL.

Once the initial state is calculated self-consistently one can calculate the pulse shape emitted by the fiber laser during Q-switching. The operation of the Q-switch is approximated by varying in time the reflectivity of the mirror positioned at $z = L_{fib}$ (Fig.9). The Q-switch is switched on for 1 μs with 100 ns transition time along a sine squared leading edge shape (Fig.10). Fig.11a shows the dependence of the signal power on time at selected positions within the cavity calculated by the 2nd order FD-MOL. The pulse peak power is approximately equal to 2 kW and the full width half maximum (FWHM) is ~ 100 ns, which are typical values for pulses generated by an erbium doped fluoride fiber Q-switched laser [6]. Fig.11b compares the dependence of the calculated pulse peak power on the spatial discretization step for both methods. These results confirm that the 2nd order FD-MOL converges much faster than the 1st order FD-MOL. In fact with the 2nd order FD-MOL the results do not vary significantly for $dz \leq 0.02$ m. In the case of the 1st order FD-MOL even at $dz = 0.004$ m the results have still not converged. Fig.11c shows the CPU time needed to obtain the results shown in Fig.11b. Again the 2nd order FD-MOL results can be obtained much faster than the 1st order ones. In fact it takes approximately 3 minutes to obtain the results using the second order FD-MOL with $dz = 0.02$ m, which is sufficient for obtaining good accuracy. For the 1st order method at $dz = 0.004$ m one needs nearly 10 hours to complete the calculations, without achieving a satisfactory accuracy. The reason for the long calculation time of the 1st order method is mainly the long time needed to calculate self-consistently the initial state of the laser. Fig.11d shows the dependence of the CPU time needed to calculate the pulse evolution only within the 1 μs temporal window set by the Q-switching pulse (c.f. Fig.10). The calculation time for the 2nd order FD-MOL is slightly larger than for the 1st order FD-MOL, which can be attributed to an additional computational overhead required for calculating numerically the FD approximations to a higher degree of accuracy.

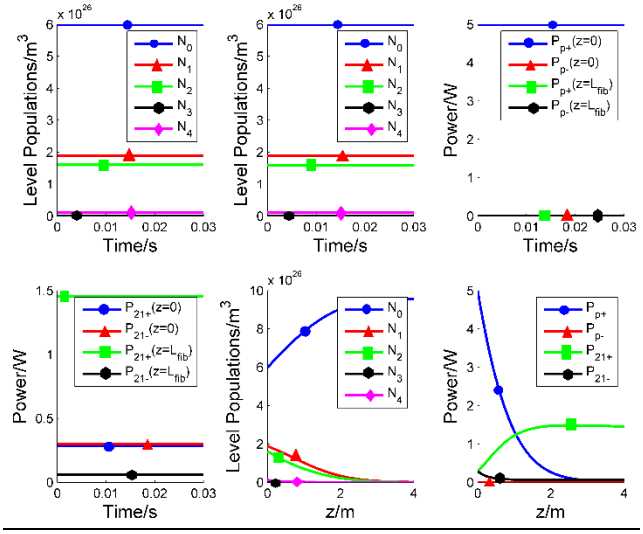

Fig. 7. Dependence on time of the level populations -a) and -b) and the pump -c) and signal power -d) at selected longitudinal positions; the final distribution of the level populations -e) and of pump and signal power -f) obtained for t = 30 ms. These results were calculated at 5 W input pump power using the 2nd order FD-MOL.

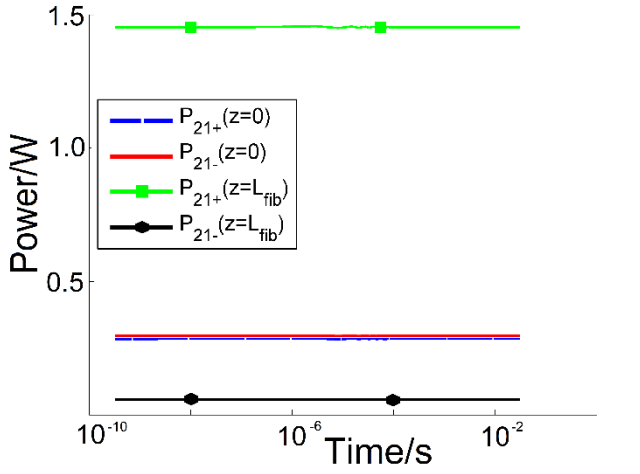

Fig. 8. Dependence of the signal power on time at selected longitudinal positions within the cavity. These results were calculated at 5 W input pump using the 2nd order FD-MOL.

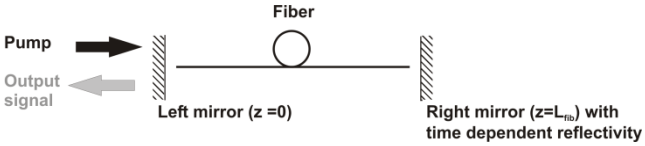

Fig. 9. Schematic diagram of a Q-switched fiber laser cavity.

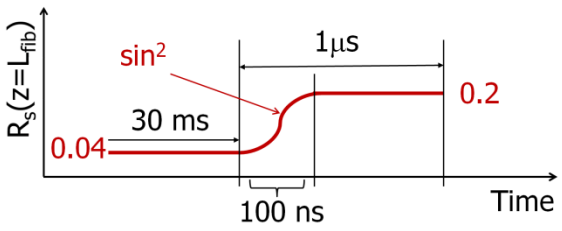

Fig. 10. Time dependence of the right mirror ($z = L_{fib}$) reflectivity.

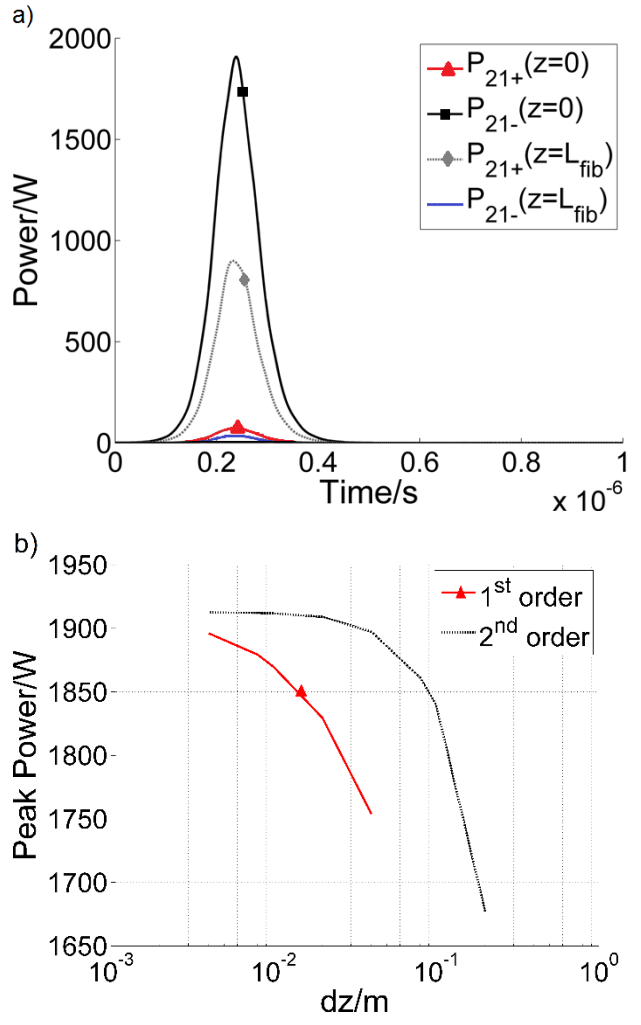

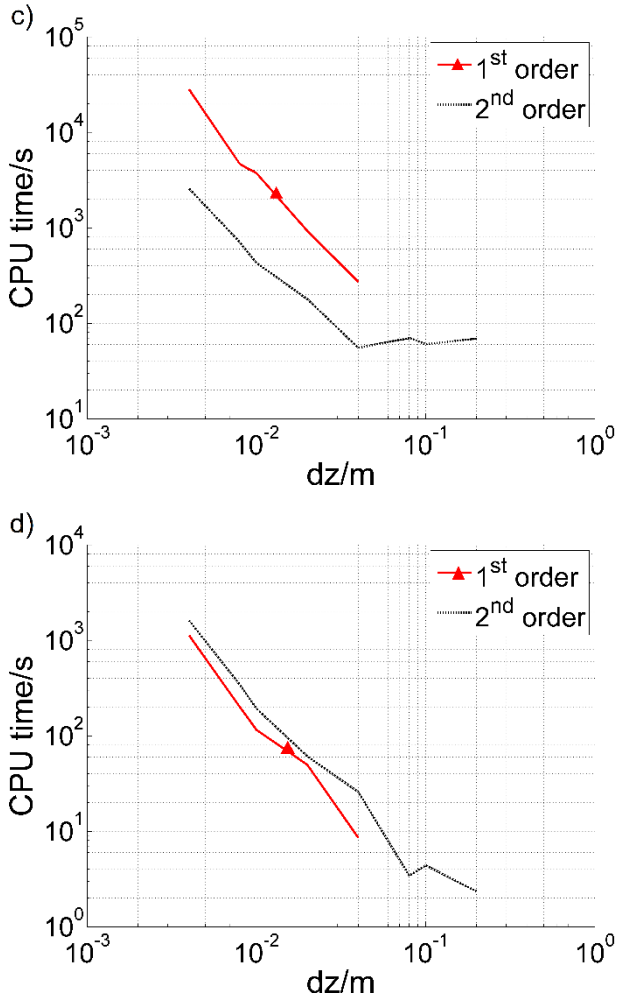

Fig. 11. Signal power pulse shape at selected positions within the cavity calculated using 2nd order FD-MOL for dz = 0.008 m -a); comparison of the dependence of signal pulse peak power on the spatial step for the 1st and 2nd order FD-MOL -b); comparison for the dependence of the overall CPU time -c) and the CPU time needed for the pulse shape calculation -d) on the spatial step for the 1st and 2nd order FD-MOL. The pump power is 15 W.

4. CONCLUSION

A method of lines for the analysis of Q-switched fluoride glass fiber lasers was developed, which is based on the finite difference method. It was demonstrated by comparing with the results obtained using the relaxation method that the developed finite difference approximation has a truly second order accuracy with respect to spatial discretization step. When compared with the standard first order FD-MOL the developed second order FD-MOL is superior both in terms of accuracy of the calculated results and the CPU time needed to complete the calculations. Unlike the time domain methods based on the method of characteristics, the developed FD-MOL can be easily implemented using the standard ODE algorithms with an adaptive step control.

References

1. J. Schneider, C. Carbonnier, and U. B. Unrau, "Characterization of a Ho^{3+}-doped fluoride fiber laser with a 3.9-μm emission wavelength," Applied Optics 36, 8595-8600 (1997).
2. S. Tokita, M. Murakami, S. Shimizu, M. Hashida, and S. Sakabe, "Liquid-cooled 24 W mid-infrared Er:ZBLAN fiber laser," Optics Letters 34, 3062-3064 (2009).
3. S. Tokita, M. Murakami, S. Shimizu, M. Hashida, and S. Sakabe, "12 W Q-switched Er:ZBLAN fiber laser at 2.8 μm," Optics Letters 36, 2812-2814 (2011).
4. D. Faucher, M. Bernier, G. Androz, N. Caron, and R. Vallee, "20 W passively cooled single-mode all-fiber laser at 2.8 mu m," Optics Letters 36, 1104-1106 (2011).
5. M. R. Majewski and S. D. Jackson, "Highly efficient mid-infrared dysprosium fiber laser," Optics Letters 41, 2173-2176 (2016).
6. S. Lamrini, K. Scholle, M. Schäfer, P. Fuhrberg, J. Ward, M. Francis, S. Sujecki, A. Oladeji, B. Napier, A. Seddon, M. Farries, and T. Benson, "High-Energy Q-switched Er:ZBLAN Fiber Laser at 2.79 μm," in CLEO/Europe-EQEC (OSA, Munich, 2015), pp. Mid-IR fiber laser systems II CJ_7_2.
7. O. Henderson-Sapir, J. Munch, and D. J. Ottaway, "Mid-infrared fiber lasers at and beyond 3.5 mu m using dual-wavelength pumping," Optics Letters 39, 493-496 (2014).
8. Darren D. Hudson, "Invited paper: Short pulse generation in mid-IR fiber lasers," Optical Fiber Technology 20(6), 631-641 (2014). http://dx.doi.org/10.1016/j.yofte.2014.08.003
9. J. Li and S. D. Jackson, "Numerical Modeling and Optimization of Diode Pumped Heavily-Erbium-Doped Fluoride Fiber Lasers," IEEE Journal of Quantum Electronics 48, 454-464 (2012).
10. J. Li, H. Luo, Y. Liu, L. Zhang, and S. D. Jackson, "Modeling and Optimization of Cascaded Erbium and Holmium Doped Fluoride Fiber Lasers," IEEE Journal of Selected Topics in Quantum Electronics 20(2014).
11. S. D. Jackson, M. Pollnau, and J. Li, "Diode Pumped Erbium Cascade Fiber Lasers," IEEE Journal of Quantum Electronics 47, 471-478 (2011).
12. M. Pollnau, "The route toward a diode-pumped 1-W erbium 3-mu m fiber laser," Ieee Journal of Quantum Electronics 33, 1982-1990 (1997).
13. M. Gorjan, M. Marincek, and M. Copic, "Role of Interionic Processes in the Efficiency and Operation of Erbium-Doped Fluoride Fiber Lasers," IEEE Journal of Quantum Electronics 47, 262-273 (2011).
14. G. Zhu, X. Zhu, R. A. Norwood, and N. Peyghambarian, "Experimental and Numerical Investigations on Q-Switched Laser-Seeded Fiber MOPA at 2.8 mu m," Journal of Lightwave Technology 32, 3951-3955 (2014).
15. M. Karasek, J. Kanka, P. Honzatko and P. Peterka, "Time-domain simulation of power transients in Raman fiber amplifiers", Int. J. Numer. Model. 17, 165-176 (2004)
16. Yong Wang, Chang-Qing Xu, "Actively Q-switched fiber lasers: Switching dynamics and nonlinear processes," Prog. Quantum Electron. 31, 131–216 (2007)
17. P. P. Vasil'ev, "High-Power High-Frequency Picosecond Pulse Generation by Passively Q-Switched 1.55 μm Diode Lasers," IEEE Journal of Quantum Electronics 29, 1687-1692 (1993).
18. S. Sujecki, "Arbitrary truncation order three-point finite difference method for optical waveguides with stepwise refractive index discontinuities," Optics Letters 35, 4115-4117 (2010).
19. S. Sujecki, "Accuracy of three-point finite difference approximations for optical waveguides with step-wise refractive index discontinuities," Opto-Electronics Review 19, 145-150 (2011).
20. S. Sujecki, "Extended Taylor series and interpolation of physically meaningful functions," Optical and Quantum Electronics 45, 53-66 (2013).
21. S. Sujecki, "A simple technique for calculation of numerical integration errors for physically meaningful functions," Afrika Matematika 25, 53-65 (2014).
22. J. K. White and J. V. Moloney, "A coupled-mode model for the Fabry-Perot semiconductor laser kink instability," IEEE Journal of Selected Topics in Quantum Electronics 9, 816-822 (2003).
23. S. Sujecki, "An Efficient Algorithm for Steady State Analysis of Fiber Lasers Operating under Cascade Pumping Scheme," Intl. Journal of Electronics and Telecommunications 60, 143-149 (2014).